Electrochimica Acta 211 (2016) 488–498

Contents lists available at ScienceDirect

Electrochimica Acta

journal homepage: www.elsevier.com/locate/electacta

Activated carbon derived from non-metallic printed circuit board waste for supercapacitor application

Raghu Raman Rajagopal[a], L.S. Aravinda[b], Ravindra Rajarao[a,*], Badekai Ramachandra Bhat[b], Veena Sahajwalla[a]

[a] Centre for Sustainable Materials Research and Technology (SMaRT), School of Materials Science and Engineering, UNSW Australia, Sydney, NSW 2052, Australia

[b] Catalysis and Materials Laboratory, Department of Chemistry, National Institute of Technology Karnataka, Surathkal, D.K., Karnataka 575025, India

ARTICLE INFO

Article history:
Received 7 April 2016
Received in revised form 28 May 2016
Accepted 15 June 2016
Available online 16 June 2016

Keywords:
Electronic waste
Waste PCBs
Activated carbon
Supercapacitors

ABSTRACT

Activated carbons (ACs) have been synthesized by using waste PCBs via physical activation subsequent to pyrolysis processes. The physical and chemical properties of the produced activated carbons were studied using nitrogen adsorption, FT-IR spectroscopy, RAMAN spectroscopy, X-ray diffraction, X-ray photoelectron spectroscopy and scanning electron microscopy techniques. Among the synthesized ACs, AC with the highest surface area of 700 $m^2 g^{-1}$ produced at 850 °C for a time interval of 5 h was subjected to electrochemical studies. Capacitance behaviour of the obtained AC sample has been evaluated using cyclic voltammetry (CV), galvanostatic charge–discharge (GC-D) measurements and electrochemical impedance spectroscopy (EIS) technique. Specific capacitance (C_{spec}) values vary from 220, 185 and 156 $F g^{-1}$ for corresponding scan rate of 30, 50 and 100 $mV s^{-1}$ respectively. The well-developed surface area properties and good capacitance values associated with nitrogen functionalities indicates the AC developed is a good and suitable candidate for the supercapacitor fabrication.

1. Introduction

Supercapacitors is one of the energy storage devices which is considered to be important due to its high power density, longer robustness, rapid charging ability and better efficiency over the rechargeable batteries [1,2]. Supercapacitors are classified into two types, based on energy storage principle; electric double layer capacitors (EDLCs) and pseudo capacitors [3]. EDLCs capacitance has its charge stored electrostatically at the electrode/electrolyte interface which depends significantly on the surface area of electrodes, which is in contact with electrolyte ions. In case of pseudocapacitors, the capacitance stores its charge depending on electron transfer between the electrolyte ion and the surfaces of the electrodes, i.e., electrodes are exposed to the fast and reversible faradaic redox reactions [4]. Recently various carbon based materials are used as electrodes for supercapacitors, which include activated carbons, mesoporous carbons, carbon nanotubes and graphene [5–7]. Carbon nanotubes and graphenes though extensively studied for supercapacitor applications has its drawback for being highly priced and tedious process involved in their production. [8]. Activated carbon is considered as the most beneficial source of supercapacitor electrode material compared to the other materials due to its following advantages; effective electrical conductivity, high surface area, longer cycling life, relatively cost effective, high capacitance, good porosity, electrochemical stability and most importantly environment friendly nature [9–11]. Activated carbon has its precursors from various resources such as carbonaceous, agricultural and industrial materials (few examples are coal, coke, peat, petroleum, wood or coconut oil palm shells, banana fibers, corn grains, lapsi seed, needle cokes, seaweeds, sunflower shells, etc.) [12–14]. Out of above mentioned examples coal, coke and petroleum sources are expensive and rapidly exhaustible with high energy consumption. Hence agriculture-industry based activated carbon attracts more attention than the expensive activated carbon produced through coal. Henceforth finding an alternative waste source apart from agro-based wastes or non-biodegradable pollutant waste as resource will provide a potential opportunity for the synthesis of activated carbon and for the application in producing electrodes for supercapacitors.

Electronic wastes (e-wastes), one of the rapidly growing waste generates around 20–50 million tonnes annually. It continues to increase at a rapid rate of around 4–5 percent per year [15,16].

* Corresponding author. Tel.: +61 2 9385 9934; fax: +61 2 9385 4292.
E-mail address: r.rajarao@unsw.edu.au (R. Rajarao).

http://dx.doi.org/10.1016/j.electacta.2016.06.077
0013-4686/

Technological innovations and the rapid production of electronics have led to an associated increase in use of electronic devices resulting in significant generation of e-waste. Utilising this e-waste as a resource will provide an effective alternative to use of conventional raw materials. In particular printed circuit boards (PCBs) are prevalent in almost every electrical and electronic gadget. PCB is a complex structure to assemble and also to dismantle, as it is built by using both metals and non-metals. PCBs are basically classified into single/double sided and multi-layered PCB. The configurational structural arrangement of parts is more complex in multilayered PCBs than in the single/double sided PCB [17–20]. PCBs in computers and communication equipment are made from glass fibre reinforced epoxy resin (referred to commercially as FR-4 type) but televisions, monitors and home electronics predominantly use PCB's made of phenolic based polymeric material (FR-2 type). Generally in PCBs the arrangement of polymers, ceramics and metals assembled and manufactured in one substrate. In recent days the fabrication of PCBs are becoming more complex with further reduction in size therefore leading to extremely tedious to recycle or to recover the materials for further usage. Pyrolysis is one of the effective ways of recovering valuable materials from e-waste compared to other conventional physico-chemical processes. Pyrolysis process involves heating the material in an inert atmosphere [21]. It is widely practiced for its ability to disintegrate the matrices of metal and non-metals in the complex designed PCB. The most common by-products produced during pyrolysis process are gas and residue [22]. Most of the research works were focussed on recovering valuable metals present in waste PCB but recycling non-metallic fractions (NMF) are neglected and landfilled again as secondary waste. Waste PCB of monitor from an End of life computer, which is considered to be polymer rich based material (FR-2) produces carbon rich non-metallic residue after pyrolysis process. Therefore, this alternative secondary waste NMF can be considered for replacing the conventional sources to produce activated carbon which helps in maintaining the much needed sustainability. This further largely helps in bringing down the environmental concerns caused through e-waste and also as an electrode material for super-capacitor.

In this present study we have devised a novel approach by utilising the NMF of PCBs as the source for activated carbon. A detailed investigation has been performed to study the morphology and composition of the activated carbon using various analytical techniques. In addition, the synthesised AC from waste PCB was used as supercapacitor electrodes. The electrochemical properties of the prepared AC were analysed using Galvanostatic charge-discharge measurements; cyclic voltammetry (CV) and electrochemical impedance spectroscopy (EIS) were used to study the electrochemical properties of the supercapacitor electrodes. This study can be demonstrated as a simple approach to synthesize AC. Further this approach will have a major effect in lessening the waste PCBs overall.

2. Experimental

2.1. Materials and methods

Random PCB of End of life monitor (polymer base material, FR-2 type) of a computer was picked up from the recycling unit of UNSW Australia, Sydney for this study. The multifarious PCB was physically dismantled from its units with the help of mechanical devices. Majority of transistors, capacitors, semiconductor circuits, battery, ceramic projections and microchips were also removed. The dismantled PCB from monitors was further truncated into possible smaller sizes (~1 cm) and then used accordingly. Homogenisation of the truncated PCB was achieved by converting them into fine powders by using CryoMill (Mixer Mill—Retsch®) grinding technique under the Liquid Nitrogen (Dewar LN2 Auto fill 501—Retsch®) atmosphere.

Raw waste PCB powders and their non-metallic residue obtained after pyrolysis were examined using PANalytical PW2400 Sequential Wavelength Dispersive X-Ray Fluorescence (XRF) spectrometry to determine the composition of various elements.

2.2. Pyrolytic approach

Pyrolysis of PCB was performed under controlled conditions of atmospheric pressure in a horizontal tube furnace in an inert (argon) atmosphere. The furnace is programmed to a predetermined temperature of 800 °C which is controlled by a thermocouple. A measured quantity of waste PCB sample was kept in an alumina crucible and then placed on to a sample holder made of graphite. Before exposing the sample to hot zone of the furnace the sample holder along with the sample is placed in the cold zone for 5 minutes to avoid thermal shock. After 20 minutes in the hot zone the pyrolysed WPCB samples were taken out and allowed to cool down in argon atmosphere to room temperature. In the obtained pyrolysed residue, the metallic fractions (MF) were easily separated manually from the non-metallic fractions. The gases generated during the pyrolytic experiments were not recovered for analysis but allowed to escape the furnace using multi point exhaust system. The obtained non-metallic fraction residues were further characterised and used to prepare activated carbon.

2.3. Preparation of activation carbon

The activation of the obtained PCB non-metallic char is achieved by using physical or chemical method. CO_2 gas was used for the activation process mainly for its purity and easy to handle properties [23]. The weighed non-metallic waste PCB char was placed in the tubular furnace and then inert atmosphere was switched to CO_2 atmosphere. It was noted prior to the experiments that CO_2 gas leakage has been checked thoroughly to avoid failure in activation. The samples were activated at 3 different temperatures, (650 °C, 750 °C and 850 °C) time intervals (3 h and 5 h) and later cooled down in an inert atmosphere. The resulting activated carbon was further for characterised.

2.4. Characterisation of activated carbon

Nitrogen adsorption isotherms were analysed by means of nitrogen adsorption at 77 K using a TriStar 3000 V6.08 A. Samples were degassed at 150 °C under vacuum for atleast 3 h prior to measurement. The multipoint Brunauer-Emmette-Teller (BET) method was used to determine the total surface area. For the mesopore surface area, pore volume and pore diameter, the Barrette-Joynere-Halenda (BJH) method was used. Micropore surface area and pore volume were determined using the t-method, and the micropore diameter was determined using the Dubinine-Astakhov (DA) method. The external surface area S_{ext} of the sample can be determined from the slope (s) of the t-plot between the relative pressure and volume adsorbed. Micropore surface area (S_{micro}) can be calculated from the relation $S_{micro} = S_{BET} - S_{ext}$ (m^2/g) Where, S_{ext} is calculated using the relation $S_{ext} = s \times 15.47$ (m^2/g).

Scanning Electron Microscope (SEM) was used to describe the physical structure of the produced activated carbon. The samples were then examined and imaged using a TM 3000 Hitachi Scanning Electron Microscope (SEM).

XPS analysis was carried out on produced activated carbon obtained by using Thermo ESCALAB250i X-ray Photoelectron

Spectrometer. The Al Kα line was used as the X-ray source. For measurements, samples were loaded into ultra-high vacuum (about 2×10^{-9} mbar) chamber of the XPS apparatus.

The crystalline components of activated carbon was analysed by PANalytical X'Pert Pro multipurpose X-ray diffractometer (XRD), operating at 40 kV and 40 mA and measurements were recorded from a start angle 2 h = 10° to an end angle of 80°, with total accumulation time of around 30 min.

A Raman spectrum was also acquired for activated carbon to determine the crystallinity and molecular structure using Renishaw Invia Raman Microscope. Spectra were measured at constant room temperature using 514 nm wavelength. The laser was focused through a microscope with a 50X objective. Raman spectra presented in this study corresponds to accumulation of 4 spectra's recorded from 800 to 1800 cm^{-1} over 30 seconds.

Fourier Transform Infrared (FTIR) spectroscopy analysis was performed to study the surface chemistry of chars. The activated carbon was powered and mixed with KBr in a mass ratio of 1:100, and then the samples was scanned using Spectrum 100, PerkinElmer Fourier transform infrared spectroscopy in the range of 4000–650 cm^{-1} to analyse the functional groups in activated carbon.

2.5. Electrode preparation and electrochemical measurements

Irrespective of the larger specific capacitance output, two-electrode system was used over the three-electrode system. Two-electrode system has sufficient potential compared to real supercapacitor configurational details. It is also learned that the major physical properties such as charge transfer, internal voltage, etc., of an ideal supercapacitor could be simulated using two-electrode system. Therefore two-electrode mechanism is more suitable than the three-electrode configuration for evaluating the supercapacitor performance measurements [24,25]. The working electrodes were fabricated using the activated carbon derived from waste PCB. The supercapacitor electrode was prepared by sandwiching two symmetric electrodes by using separator in aqueous electrolyte. Before assembly, separator sandwiched between the electrodes was rinsed with H_2SO_4 and the whole system was locked with the stainless steel clamps.

The electrochemical properties of the supercapacitor electrodes were studied using cyclic voltammetry (CV), galvanostatic charge–discharge (GC-D) measurements and electrochemical impedance spectroscopy (EIS) on Autolab Potentiostat/Galvanostatic (Model-PGSTAT 30, Ecochemie, The Netherlands) electrochemical workstation.

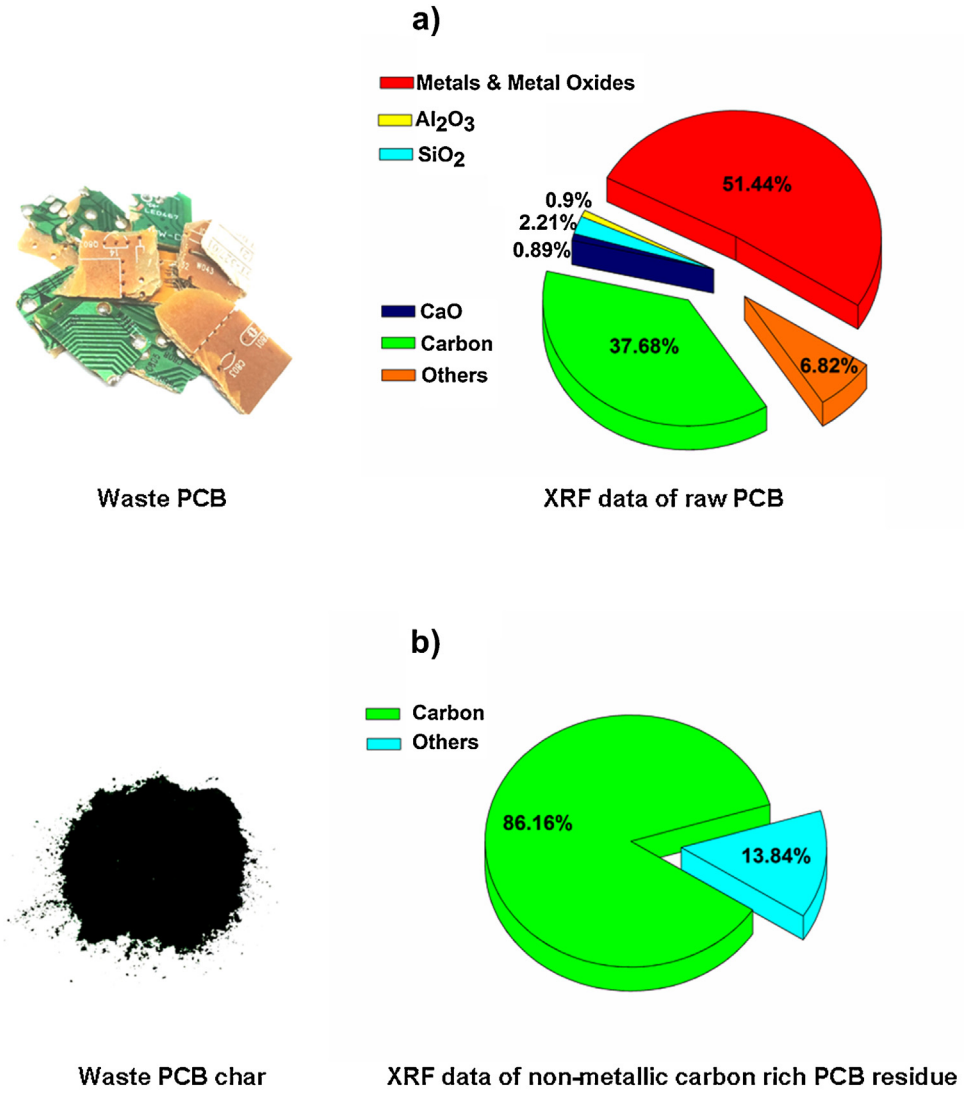

Fig. 1. XRF analysis data of a) raw waste PCB and b) non-metallic PCB residue.

3. Results and Discussion

3.1. Characterisation of waste PCB and non-metallic residue

PCBs are key component of all electrical and electronic components. Generally, PCB components can be divided broadly into Metallic fractions (MFs) and Non-metallic fractions (NMFs). PCB is composed of metallic portions such as copper, tin, iron; and major composition of non-metals as plastics, epoxy resins, glass fibers; The XRF analysis of raw waste PCB as shown in Fig. 1 **a** confirms the generic description of PCB with metals dominating the composition with 51%. The polymer based waste PCB contributes to the presence of carbon with the composition around 38%. The compositions of alumina (0.9%), silica (2.21%) and calcium (0.89%) confirm the presence of glassfibers with the remaining 7% contributes to the additives and other components present in the sample.

Thermogravimetric analysis (TGA) provides the knowledge of pyrolysis of waste PCB. TGA graph clearly indicates that the major decomposition of waste PCB happens between 250 °C–380 °C temperature range. The complete degradation of all organic matter happens until 700 °C–800 °C. Therefore the temperature 800 °C was chosen for the waste PCB pyrolysis experiments.

Pyrolysis of waste PCB under controlled conditions yields a solid residue consisting of pyrolyzed pieces of the PCB board which could be crumbled with minimal manual pressure. Apart from the boards and other impurities the residue could be then easily separated to MF and NMF as shown in Fig. 2. In general, NMF is predominantly composed carbon and ceramics, along with some metal impurities [15]. XRF studies of NMF obtained after pyrolysis consists of 86% carbon, 1.5% nitrogen and 10.5% of other related fractions Fig. 1 **b** respectively. From the result, it is clearly evident that because of the high yield of carbon the non-metallic waste PCB residue can be utilised as a raw material for synthesis of activated carbon.

3.2. Characterisation of activated carbon

3.2.1. N_2 adsorption isotherm in activated carbon

Fig. 3 **a** shows nitrogen adsorption-desorption isotherms of activated carbon derived from waste PCB by physical activation process using CO_2 gas at various activation time and temperatures. Based on the IUPAC data classification, the obtained isotherms for the activated carbon samples exhibit a type I, IV and V patterns [26], showing combination of both microporous and mesoporous characteristics. The volumes of the adsorbed nitrogen of the isotherm curves are relatively low. Further it shows a sharp increase in adsorption at low relative pressure indicating that nitrogen molecules are adsorbed predominantly in the microporous regions of activated carbon. A slip-knee stage is also observed during the transition phase of relative pressure (ρ/ρ_o) to saturated stages, indicating the curves are showing a narrow pore size distribution. From the results, it is observed that the quantity of volatiles released during decomposition and pore formation is higher at higher temperatures at different time intervals resulting in increase of surface area. The hysteresis cycles observed in the adsorbed isotherm curves shows that are a general property of capillary condensation in mesoporous solids. Hysteresis loop

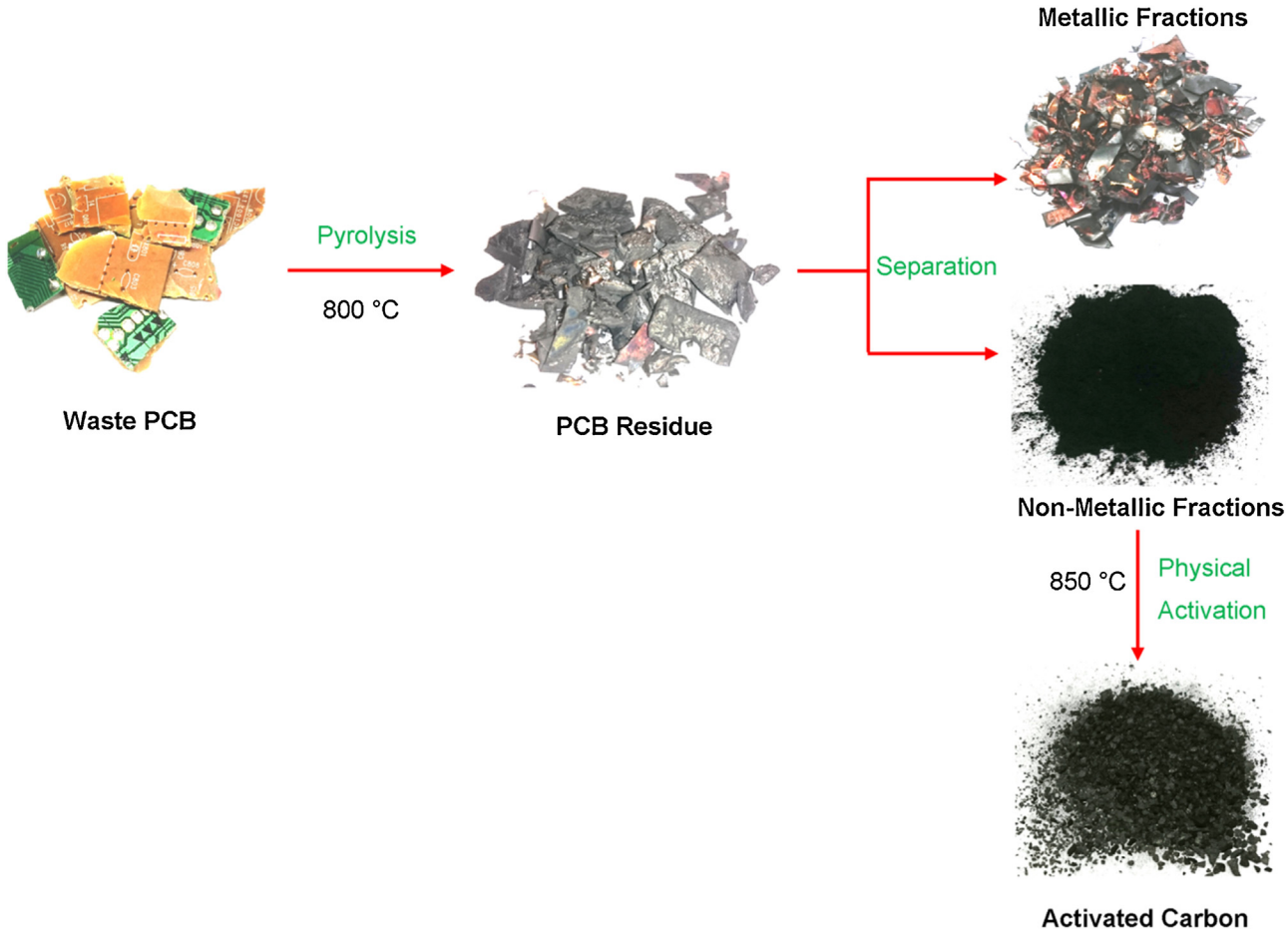

Fig. 2. Schematic representation of synthesis of activated carbon form waste PCB.

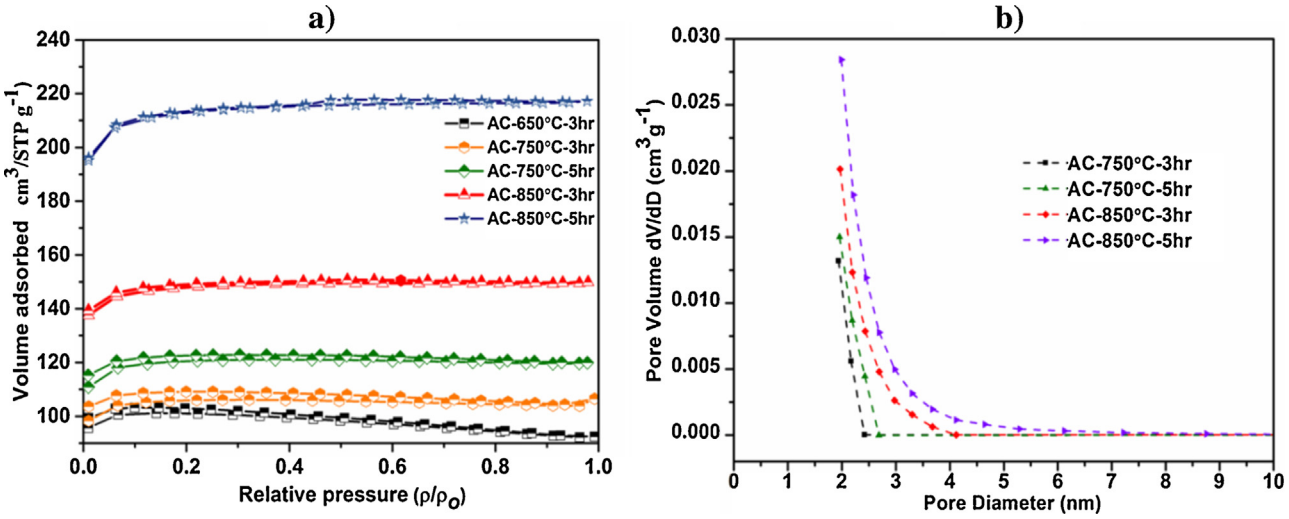

Fig. 3. Nitrogen adsorption/desorption isotherms for prepared activated carbons at various duration and temperatures. b) Nitrogen adsorption/desorption pore size distributions.

determines the average size of the micropore, if the curvature is opening then the size of the micropores is large, implying that the activated carbon generated contain predominantly microporous with small amounts of mesopores [27].

Table 1 summarises the total, micropore and external surface areas including the pore volume and average pore size. The BET surface area (S_{BET}) increases from 316 to 700 m^2/g and total pore volume increases from 0.003 to 0.022 $cm^3\,g^{-1}$, likewise micropore surface area (S_{mic}) and external surface area (S_{ext}) also follows the similar trend. Activation process influences the improvement of porosity characteristics with the increase in pore diameter as shown in Fig. 3 **b**. It can be observed that the increase in temperatures and increase in the activation time from 3 to 5 hours increases the surface area due to the development of pores in samples during activation process. Activated carbon obtained at 850 °C for a time period of 5 hours shows highest amount of activation corresponding to the quantity of N_2 adsorbed in adsorbent, therefore having the highest specific surface area, (S_{BET} = 700 m^2/g) in comparison to the other samples and also the highest pore volume of 0.022 $cm^3\,g^{-1}$.

Deformation of the pores and its influences towards the increase and decrease of the average pore size depends totally on the activation hours. The average pore diameter obtained for an activated time of 3 hours at 650 °C is 2.16 nm which increases to 2.62 nm with the increase in temperature to 750 °C. However, with the same 750 °C temperature the average pore diameter decreases to 2.41 nm which may be due to the micropore deterioration caused by increasing the activation hours from 3 to 5 and may result in the formation of mesopores. On the other hand the average pore diameter resulted at 850 °C for the activation time of 3 and 5 hours increases from 2.39 nm and 2.64 nm respectively. This phenomenon also may explain the breakage of the micropore walls and the transforming into mesopore surface (>2 nm) at elevated temperatures and at higher activation hours. Therefore activated carbon obtained at 850 °C for an activation time of 5 hours has higher surface properties in comparison to the other samples.

3.3. XPS analysis

XPS investigation is performed in order to study the surface chemistry of carbon structure involved in the prepared activated carbon at 850 °C for 5 hours. Data is recorded with the pass energy of 100 eV for the survey scans and 20 eV for the region scans of C1s and N1s. By calibrating the binding energies (BE) the samples were charged on the graphitic carbon C1s peak at BE 285 eV. In order to get good spectra the C1s and N1s were analysed by curve fitting. Fig. 4 **a** shows the survey scans of carbon (C1s), nitrogen (N1s) and oxygen (O1s) peaks with BE of 284.40 eV, 400 eV and 533 eV respectively. Fig. 4 **b** shows the high resolution XPS spectra of C1s for the AC-5h–850 °C sample. For the investigated sample, the deconvolution of C1s spectrum gives at least seven forms of carbon peaks occurring on surface confirming the presence of carbon can be determined. These seven peaks are related to C=C bonds (284.64 eV), C—C bonds (285.0 eV), C—O bonds (286.48 eV), C=O bonds (287.88 eV), COO bonds (288.98 eV), O—C=O bonds (290.38 eV) and finally π-π transition (291.88 eV) respectively [28,29] (Table 2). The bonds C, C—O, C=O and COO fractions of the C1s spectrum are 41.65%, 31.2%, 8.18 and 3.14% in AC-5h–850 °C sample respectively, indicating a significant presence of oxygen – containing functional groups.

The N1s region spectrum can be deconvoluted to four peaks as shown in Fig. 4 **c**, which corresponds to four nitrogen functional group types, such as pyridinic (N1s-B, 398 ± 0.3 eV), pyrrolic or pyridonic (N1s-C, 400.3 ± 0.3 eV), quaternary nitrogen (N1s-A, 401 ± 0.3 eV) and pyridine-N-oxide (N1s-D, 403 ± 0.3 eV) [30].

Table 1
Surface texture measurements of prepared activated carbons.

Carbonisation temperature	S_{BET} (m^2g^{-1})	S_{mic} (m^2g^{-1})	S_{ex} (m^2g^{-1})	Slope $\frac{(\rho/\rho_0)}{V}$	V_t (cm^3g^{-1})	a (nm)
AC-3–650 °C	316	309	7	0.427	0.003	2.16
AC-3–750 °C	340	324	16	1.024	0.006	2.62
AC-5–750 °C	386	348	38	2.468	0.008	2.41
AC-3–850 °C	476	387	89	5.725	0.013	2.39
AC-5–850 °C	700	512	179	11.565	0.022	2.64

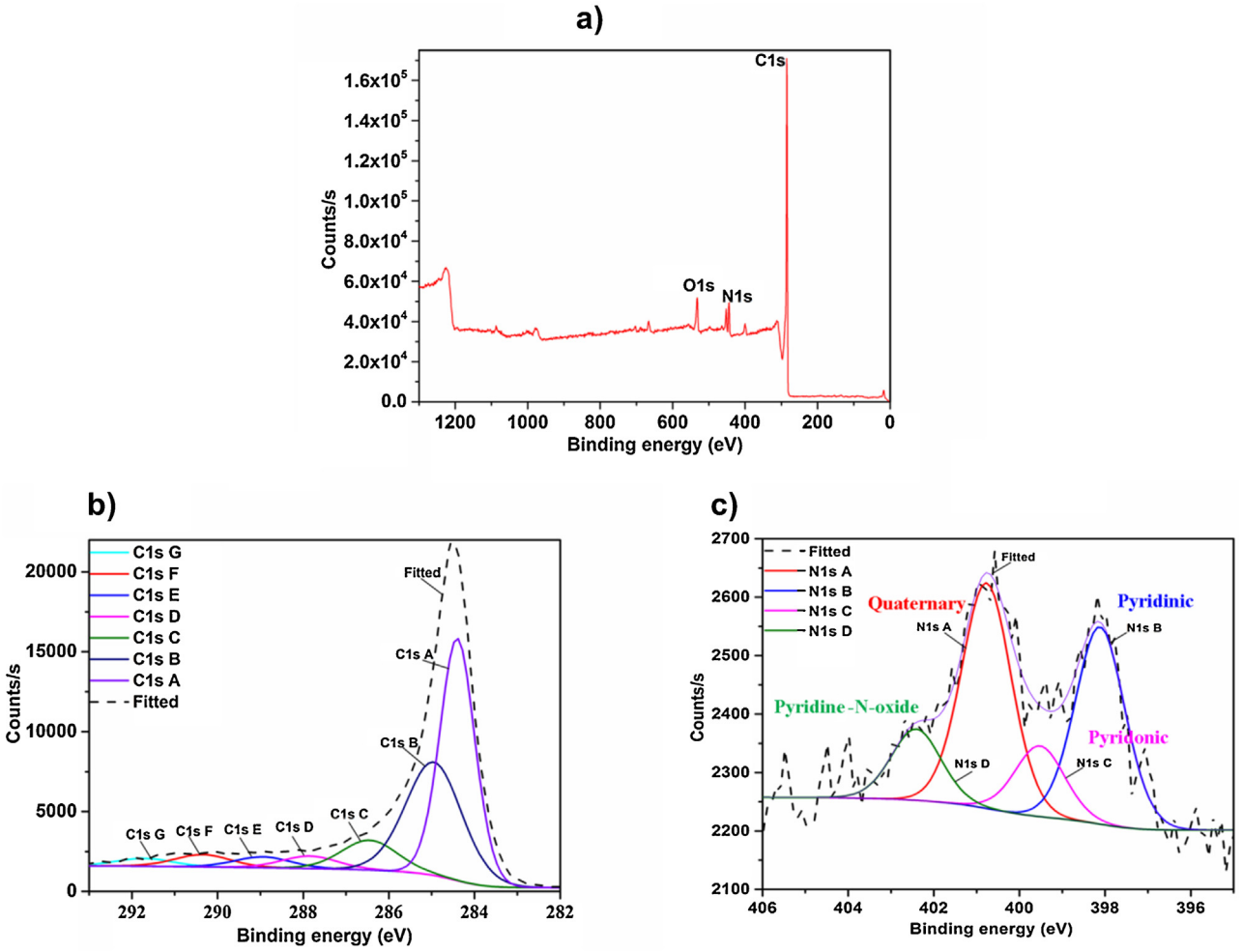

Fig. 4. a) Survey peaks b) C1s and c) N1s XPS spectra of prepared activated carbon at 850 °C, 5 h.

Table 2
XPS peak positions of fitted C1s and N1s at 850 °C.

Name	Start BE	Peak BE	End BE	FWHM (eV)	Area (P) CPS eV)	Atomic %
C1s A	294.18	284.40	281.38	0.96	15813.93	41.65
C1s B	294.18	284.95	281.38	1.54	11845.55	31.2
C1s C	294.18	286.45	281.38	1.54	3104.25	8.18
C1s D	294.18	287.85	281.38	1.54	1295.66	3.41
C1s E	294.18	288.95	281.38	1.54	1137.55	3
C1s F	294.18	290.35	281.38	1.54	1286.75	3.39
C1s G	294.18	291.72	281.38	1.54	820.36	2.16
N1s A	405.98	400.77	394.78	1.37	571.2	0.85
N1s B	405.98	398.12	394.78	1.37	499.88	0.74
N1s C	405.98	399.52	394.78	1.37	179.45	0.27
N1s D	405.98	402.41	394.78	1.37	180.8	0.27

N1s-B is pyridinic N which refers to the N bonds to two carbon atoms in a six-membered ring at the edge of the graphene layer. On the other hand N1s-C represents pyrrolic N in a five-membered ring incorporated with the phenolic or carbonyl group to the neighbour carbon atoms of the ring. Finally, the N1s-A is the quaternary N in which the N bonds to three carbon atoms and positions itself in the central or valley positon of the graphene layer. The content of nitrogen and its functional group types have significant effect on the capacitive performance over the super-capacitors. The pyridinic and pyrrolic nitrogen contributes significantly for energy storage performance compare to quaternary nitrogen [31,32]. The nitrogen groups also play an important role in improving the hydrophilicity and wettability of material and enabling easy accessibility of electrolyte ions [9]. The higher exposure of N1s-B and N1s-C sites than the N1s-A indicates the initial presence of electrochemical active sites for capacitance interaction. These active sites further initiate higher specific capacitor performance for the activated carbon prepared at 850 °C for 5 hours. The qualitative identification of the functional groups determined in XPS is examined and cross referred using FT-IR spectroscopy.

3.4. FTIR analysis

Fig. 5 shows the FT-IR spectra of the waste PCB and AC-5h–850 °C sample over the range of 4000–750 cm^{-1}. The evolution of the chemical compositions of the AC-5h–850 °C sample obtained from waste PCB reveals the functional groups with the presence of peaks. The Waste PCB sample shows more peaks than that found in the obtained activated carbon sample. This indicates the decomposition of few oxide groups subjected to activation at high temperatures have taken place, therefore activation process was successful. Adsorption peaks of the stretching vibrational modes obtained for AC-5h–850 °C sample mostly disappeared during the course of physical activation process. Functional groups present in the waste PCB spectrum were decomposed and vaporised as volatile materials at high temperatures. Waste PCB shows its absorption peak around 3344 cm^{-1} which shows the presence of O—H stretching vibrating band. Similarly the peaks at 2924 and

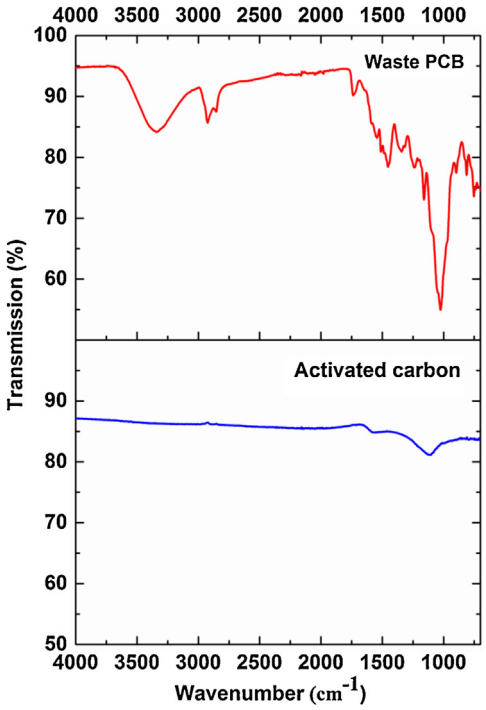

Fig. 5. FTIR spectra of waste PCB and obtained activated carbon at 850 °C.

2855 cm^{-1} denotes the existence of C—H vibrations. While the bands shifting around 1736 cm^{-1}, 1626 cm^{-1}, 1541 cm^{-1}, 1448 cm^{-1} and 1347 cm^{-1} attributes the presence of C=O/C=C stretching vibrations. Finally the broad peak around 1140 cm^{-1} shows the essential C—O—C functional group stretching mode. In case of deformed AC obtained from WPCB the peaks 2927 cm^{-1}, 1675 cm^{-1} and 1128 cm^{-1} s confirms the presence of C—H, C—O/C=C and C—O—C functional groups respectively. The oxygen (C—O, C=O) containing vibrational modes of the peaks in existence can have a substantial effect on the electrochemical behaviour of the super-capacitors.

3.5. X-Ray diffraction and Raman analysis

The structural ordering of AC obtained by waste PCB at 850 °C for 5 h was investigated by XRD. Fig. 6**a** shows the XRD pattern and two peaks were observed over the examined range (10–90°), corresponding to graphite (002) and (100) peaks respectively. Generally (002) peak is attributed to stacking of the graphitic basal planes and theoretically (002) peak is symmetric in nature. But the observed (002) peak in AC spectra is asymmetric at low scattering angles which is due to presence of γ-band. The γ-band is associated with disordered carbons such as amorphous carbon and aliphatic side chains. The (002), (001) and γ-peak in spectra indicate the presence of ordered and disordered carbon structures in the AC [33]. The Raman spectrum of AC was recorded between 800–2000 cm^{-1} and two strong peaks at 1583 cm^{-1} (G-band) and 1345 cm^{-1} (D-band) were observed respectively (Fig. 6**b**). The visible excitation always resonated with the π states, hence sp^2 sites dominates the Raman spectra of AC sample. For hexagonal graphite, 'G band' is assigned to E_{2g} vibrational mode, which is attributed to in plane stretching motion pairs of carbon sp^2 atoms. 'D band' originates due to existence of disorder in graphitic structure which is assigned to A_{1g} symmetry and peak hides under valley between two peaks, which reflects the presence of amorphous carbon. In this study, the I_V/I_G ratio (I_V is intensity of

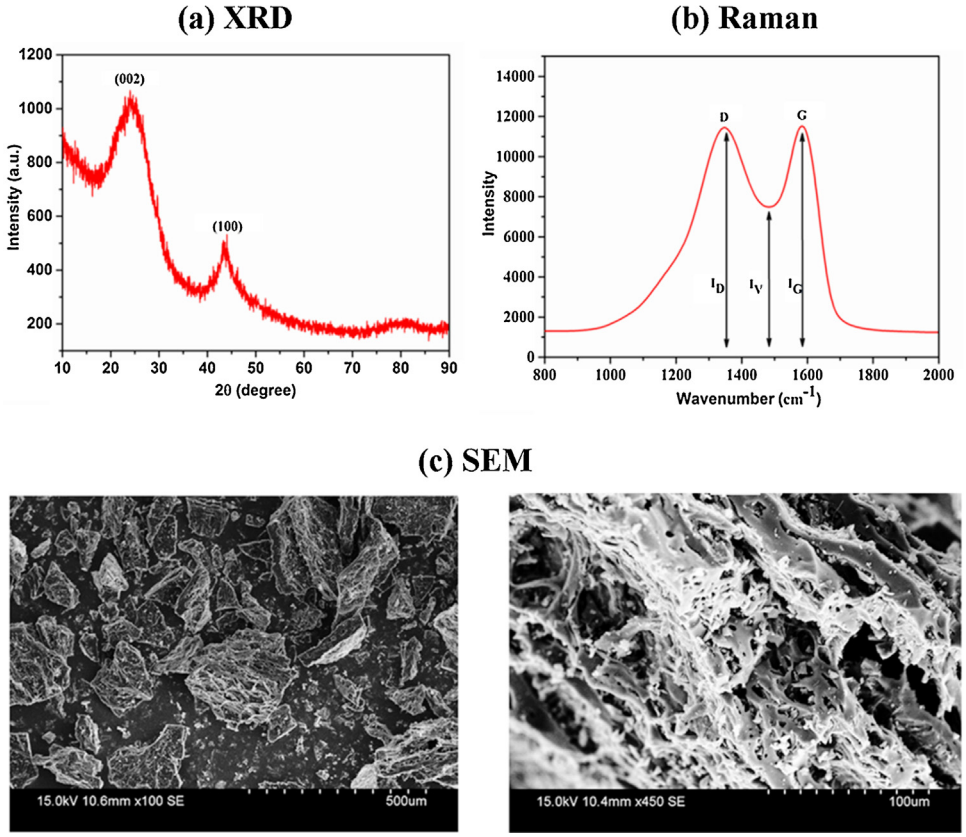

Fig. 6. a) XRD pattern of prepared activated carbon at 850 °C, 5 h b) Raman spectrum of prepared activated carbon at 850 °C, 5 h (c) Low magnification and high magnification SEM images of obtained activated carbon at 850C, 5 h.

a valley between G and D bands and I_G is intensity of G band) is been used as an indication to measure the degree of disorder and proportion of amorphous carbon. I_V/I_G (I_G—intensity of G-band and I_V—intensity of a valley between G and D bands) is 0.62, which specifies the presence of sp^2 carbons and amorphous content [34].

3.6. SEM analysis

Surface morphologies through the SEM images at low and high magnification obtained for activated carbon at 850 °C (5 h) are shown in Fig. 6**c**. The activated carbon sample at high magnification shows the lot of tunnel shaped homogenous porous structure morphologies, which is significant for both adsorption and charge storage phenomena. The pores and vesicles are clearly evident and this is well accordance with other results confirming the decomposition mechanism at activated temperatures. The pore matrix shown were the results of volatile gases escaping during the decomposition of waste PCB. The presence of pores is the important reason for the sample to incorporate active surface area. The low magnification image shows the few macropores indicating the dominance of micropores present in the sample.

3.7. Electrochemical analysis

The CV curves taken at the three different scan rates for waste PCB derived AC at 850 °C (5 h) is shown in Fig. 7**a** are fairly rectangular in shape indicating the capacitance behaviour from the formation of an electric double layer. Further the sample also exhibit strong peaks at 1 V potential and indicates that the retainment of the rectangular shape from 30 to 100 mV s^{-1} confirms the consistency of the capacitance behaviour prevailing, irrespective of the change in voltage potential [35]. This approximate symmetrical nature of CV loops indicates faster ion transport and hence better rate capability.

The gravimetric specific capacitance, C_{sp} (F g^{-1}), from the CV curves was calculated according to following equation [36].

$$C_{sp} = \frac{2(Q_+ + |Q_-|)}{2m\Delta V} \quad (1)$$

Where Q_+ and Q_- are the integrated charges of anodic and cathodic potential respectively, the m is the mass of each electrode; ΔV is the potential window (1 V in this work).

4.1. Electrochemical characterisation

Galvanic cycling and its discharge (GC-D) curves can be used to illustrate the behaviour of capacitance and its resistance. Fig. 7 **b** shows the GC-D curves measured at various applied currents 3, 4 and 5 A g^{-1} respectively. The charge and discharge curves were found to be almost symmetric, exhibiting ideal capacitive behaviour, which is a typical normal characteristic of an ideal capacitor with good electrochemical phenomena. The specific capacitance (C_s) was evaluated by chronopotentiometry according

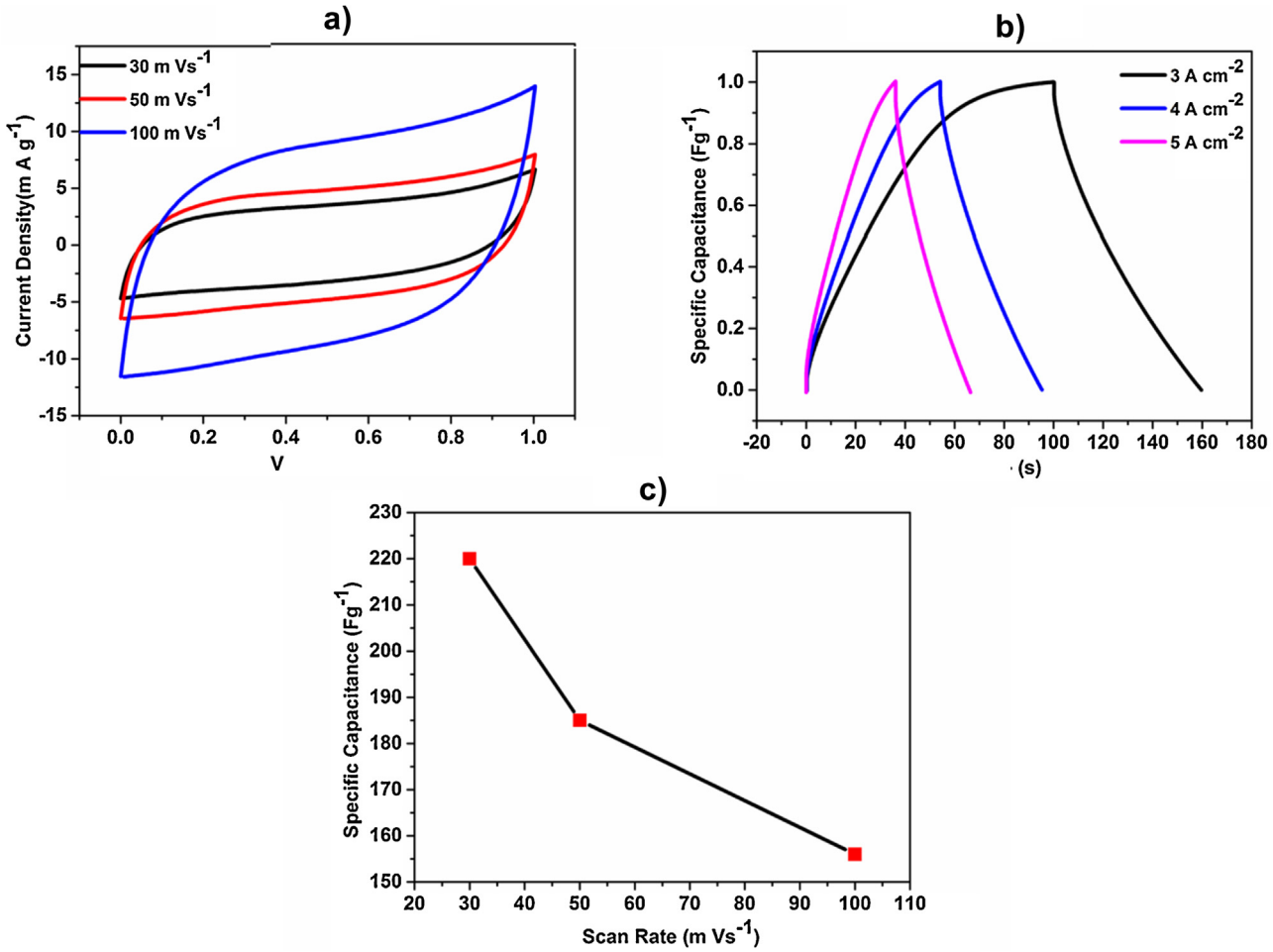

Fig. 7. a) CVs of AC electrodes at 30, 50 and 100 mV S^{-1}; b) The galvanostatic charge-discharge curves measured at 3, 4 and 5 A cm^{-2} for AC-5h–850 °C at a current density of 1 A g^{-1}; c) dependence of C_s on the scan rate of CV.

to the following equation (2).

$$C_s = \frac{2 \times C_{cell}}{m} \quad (2)$$

Where,

$$C_{cell} = \frac{I}{\left(\frac{\Delta V}{\Delta t}\right)} \quad (3)$$

Where I is the discharge current, m is the mass of material at each electrode and $\Delta V/\Delta t$ is the slope of the discharge curve (after correcting for iR drop). A factor of 2 is incorporated due to symmetric capacitor assembly of the material. The stability of the electrode was determined by cycling studies carried at constant current density of 5 mA cm^{-2} in the Voltage window of 0–1.5 V. It was observed that the specific capacitance was retained up to 98% even after 1000 cycles. This indicated that the electrode material have good stability. The specific capacitance based on the BET surface area is also calculated (Table 3) using the following relation;

$$C_{BET} = \frac{C_{s(Fg^{-1})}}{S_{BET(m^2g^{-1})}} \quad (4)$$

Where, S_{BET} is the specific surface area of the electrode. In addition to the above calculations energy density (E) and power density (P) calculation were also calculated using the relations given below:

$$E = \frac{C_s * \Delta V^2}{2} \quad (5)$$

$$P = \frac{I * \Delta V}{2 * m} \quad (6)$$

Where, energy density is expressed in watt-hours per kilogram (W h kg^{-1}) and power density in Watts per kilogram (W kg^{-1}).

At scan rate values of 30, 50 and 100 mV s^{-1} and its corresponding specific capacitance values (Fig. 7**c**) for the activated carbon sample are found to be 220, 185 and 156 F g^{-1} respectively. It is evident from the result that higher the density, lower the specific capacity which is due to the electrode polarization [37]. Cyclic stability of the sample derived, demonstrates the practical potential of the supercapacitor devices. The cyclic stability to its retention percentage plot for 1000 cycles is shown in Fig. 8**a**. From the data it is determined that the retention percentage remains approximately consistent until 100–500 charge-discharge cycles. This behaviour as in the plot suggests excellent higher rate electrochemical characteristics in energy storage application [38] through the obtained activated carbon sample from waste PCB.

According to the equation (3) the energy density of the supercapacitors determined is proportional to the specific capacitance values. According to Fig. 8**b** the power density increases with the increase in current density with the decrease in energy density values. The energy and power density derived using Ragone plot were calculated from the GC-D curved and from the equations (5) and (6). Commercially available supercapacitor based on activated carbons normally shows the energy density values ranging from 4–5 W h kg^{-1} with the power density values of 1–2 kW kg^{-1} [39].

Table 3
Capacitance measurements based on mass and surface area.

Current Density (A g^{-1})	C_{spec} (F g^{-1})	C_{BET} (F m^{-2})
30	220	0.314
50	185	0.264
100	156	0.222

Activated carbon synthesised at 850 °C for 5 h shows good performance with high energy density of 15.84 W h kg^{-1} at 850 W kg^{-1} which gradually reduces to 11.23 W h kg^{-1} at 2142 W kg^{-1}. This shows that the electrode of the AC–850 °C–5 h sample exhibits energy and power densities equivalent to the commercially available supercapacitors.

The electrochemical impedance spectroscopy (EIS) measurements were carried out over the frequency range from 100 KHz to 10 MHz. Fig. 8**c** shows the Nyquist plots and the fitting results. Information in regards to electrical conductivity, charge transfer and mass diffusion behaviour can also be obtained through EIS measurements. EIS data were analysed using Nyquist plots, which show the frequency response of the electrode/electrolyte system and are the plots of the imaginary component (Z") of the impedance against the real component (Z'). The Nyquist plot for the electrodes, show a straight line in the low-frequency region and small arc in the high frequency region which is typical supercapacitor behaviour. The arc or semi-circle region created at the higher frequency should be related to the Faradaic process of the charge-transfer at the electrode/electrolyte interface, and the resulting slope of lines at the lower frequency region should be assigned to the diffusion of the electrolyte ions in the electrolyte pores [38,37,40].

Therefore, it can be concluded that the electrode materials obtained with porous structures exhibits low ionic resistance inside which facilitates fast diffusion of the electrolyte ions in to the porous network. The equivalent series resistance (R_{ESR}) is denoted by the intersection of the curve at the real part represented by Z' in the high frequency. R_{ESR} is a combinational resistance of ionic resistance of the electrolyte, intrinsic resistance of substrate and constant resistance between electrode and current collector [41]. Table 4 shows the comparative chart of different sources through which activated carbon can be derived with its corresponding surface area and specific capacitance values. It is understood that surface area of AC produced through e-waste is higher than waste newspaper and willow catkins. On the other hand, waste sources like seed and coconut shells have higher surface area than e-waste however with specific capacitance values ranging similar around 220–234 F g^{-1}.

5. Conclusion

In summary, rapidly increasing and environmentally concerned toxic waste PCBs are used as raw material source to produce high value ACs by physical activation process for good performance supercapacitor electrodes.

- Higher activation temperature with higher time interval leads the carbonaceous material with the higher surface area (700 m^2 g^{-1}) and higher volume (0.022 cm^3 g^{-1}).
- Nitrogen adsorption (BET) and XPS techniques exhibits necessary nitrogen and carbon functional group of the synthesized AC sample which in turn supports promising capacitance behaviour.
- The specific capacitance of the chosen AC is 220 F g^{-1} at the current density of 30 mV s^{-1} and 156 F g^{-1} even at 100 mV s^{-1} with the retention value of 98% over 1000 cycles.

In conclusion, this study presents an effective approach for generating value-added activated carbon from waste printed circuit PCB boards exhibiting electrochemical behaviour suitable for energy storage applications.

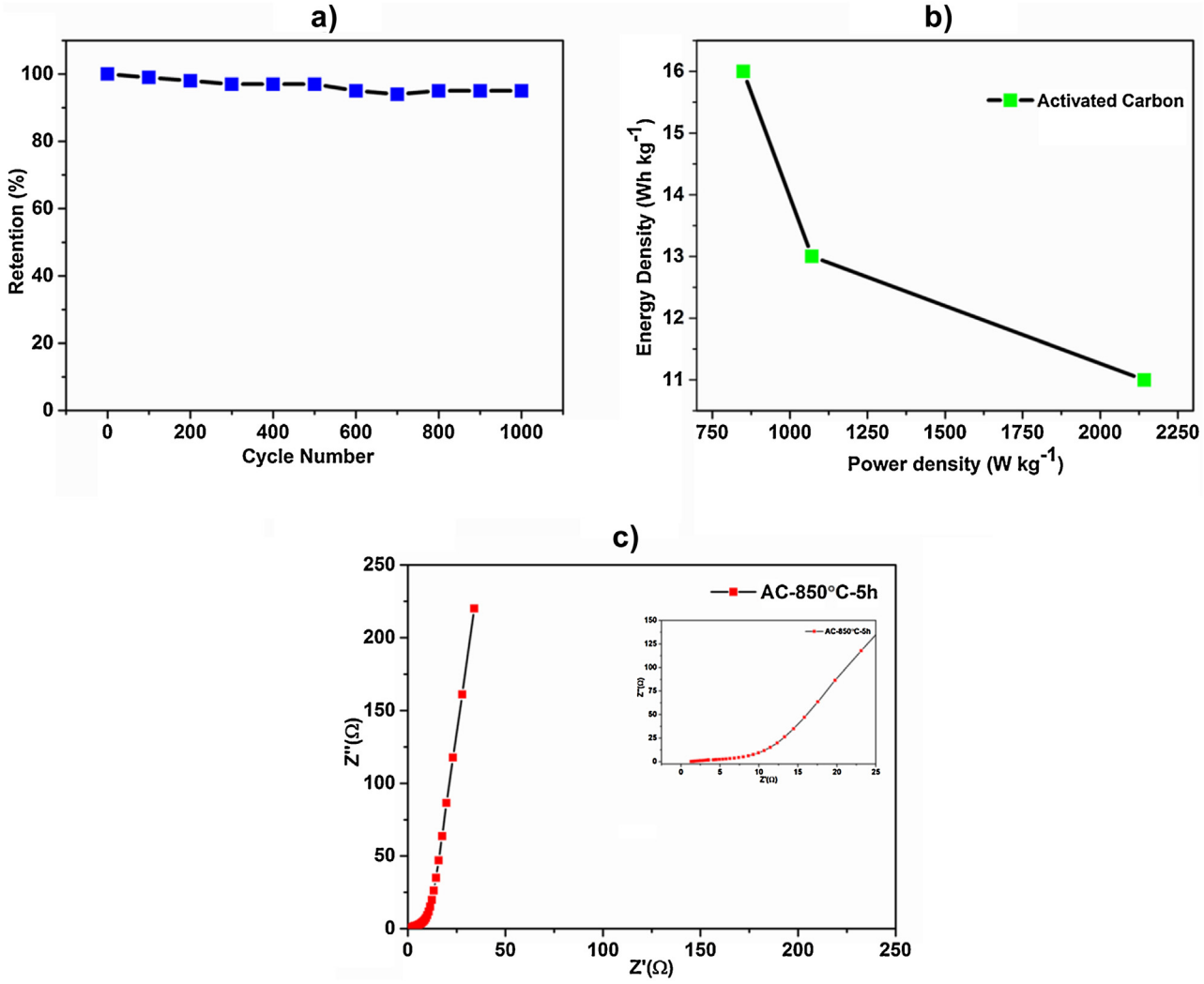

Fig. 8. a) Charge-discharge cycling stability of AC-5h–850 °C; b) Ragone plots of the energy density and power density of the AC sample; c) Nyquist plot of AC electrodes, Inset: a magnified portion at high frequency regions.

Table 4
Comparison chart of activated carbon prepared using various wastes for supercapacitors.

Material	S_{BET} ($m^2 g^{-1}$)	C_{spec} ($F g^{-1}$)	Ref.
Waste news paper	416	180	[42]
Willow catkins	645	279	[9]
Waste particle board	1758	263	[45]
Electronic waste [PCB]	700	220	This work
Argania Spinosa/seed shells	1279	234	[13]
Waste Tyre	1069	313	[46]
Coconut shell	1532	228	[43]
Waste tea leaves	2245	330	[44]

References

[1] P.J. Mahon, G.L. Paul, S.M. Keshishian, A.M. Vassallo, Measurement and modelling of the high-power performance of carbon-based supercapacitors, J. Power Sources 91 (2000) 68.
[2] L. Beihu, X. Zuoan, Z. Hua, X. Wei, W. Wenlong, W. Dihua, Enhanced capacitive properties of commercial activated carbon by re-activation in molten carbonates, J. Power Sources 298 (2015) 74.
[3] A. Burke, Ultracapacitors: why, how, and where is the technology, J. Power Sources 91 (2000) 37.
[4] Z. Li, Z. Xu, X. Tan, H. Wang, C. Holt, T. Stephenson, Mesoporous nitrogen-rich carbons derived from protein for ultra-high capacity battery anodes and supercapacitors, Energy Environ. Sci. 6 (2013) 871.
[5] W. Dewei, F. Guoli, X. Tong, M. Jinfu, G. Guihong, A melt route for the synthesis of activated carbon derived from carton box for high performance symmetric supercapacitor applications, J. Power Sources 307 (2016) 401.
[6] D.T. Pham, T.H. Lee, D.H. Luong, F. Yao, A. Ghosh, V.T. Le, T.H. Kim, B. Li, J. Chang, Y.H. Lee, Carbon Nanotube-Bridged Graphene 3D Building Blocks for Ultrafast Compact Supercapacitors, ACS Nano 9 (2015) 2018.
[7] B.E. Wilson, S. He, K. Buffington, S. Rudisill, W.H. Smryl, A. Stein, Utilizing ionic liquids for controlled N-doping in hard-templated, mesoporous carbon electrodes for high-performance electrochemical double-layer capacitors, J. Power Sources 298 (2015) 193.
[8] L. Weinstein, R. Dash, Supercapacitor carbons, Mater. Today 16 (2013) 1069.
[9] K. Wang, N. Zhao, S. Leo, R. Yan, X. Tian, J. Wang, Y. Song, D. Xu, Q. Guo, L. Liu, Promising biomass-based activated carbons derived from willow catkins for high performance supercapacitors, Electrochim. Acta 166 (2015) 1.
[10] Y. Huang, S. Candelaria, Y. Li, Z. Li, J. Tian, L. Zhang, G. Cao, Sulfurized activated carbon for high energy density supercapacitors, J. Power Sources 252 (2014) 90.
[11] E.Y.L. Teo, L. Muniandy, E. Ng, F. Adam, A.R. Mohamed, R. Jose, K.F. Chong, High surface area activated carbon from rice husk as a high performance supercapacitor electrode, Electrochim. Acta 199 (2016) 110.
[12] S. Joshi, L.K. Shrestha, Y. Kamachi, V. Malgras, M.A. Pradhananga, B.P. Pokhrel, T. Nakato, R.R. Pradhananga, K. Ariga, Y. Yamauchi, Synthesis and characterizations of nanoporous carbon derived from Lapsi (*Choerospondias axillaris*) seed: Effect of carbonization conditions, Adv. Powder Technol. 26 (2015) 894.
[13] A. Elmouwahidi, Z. Zapata-Benebithe, F. Carrasco-Marin, C. Moreno-Castilla, Activated carbons from KOH-activation of argan (Argania Spinosa) seed shells as supercapacitor electrodes, Bioresour. Technol. 111 (2012) 185.

[14] D. Wang, Z. Geng, B. Li, C. Zhang, High performance electrode materials for electric double-layer capacitors based on biomass-derived activated carbons, Electrochim. Acta 173 (2015) 377.
[15] R. Rajarao, V. Sahajwalla, R. Cayumil, M. Park, R. Khanna, Novel approach for processing hazardous electronic waste, Proc. Environ. Sci. 21 (2014) 33.
[16] J. Cui, E. Forssberg, Mechanical recycling of waste electric and electronic equipment: a review, J. Hazard. Mater. 99 (2003) 243.
[17] R.R. Rajagopal, R. Rajarao, V. Sahajwalla, High temperature transformations of waste printed circuit boards from computer monitor and CPU: Characterisation of residues and kinetic studies, Waste Manage. (online) (2016), doi:http://dx.doi.org/10.1016/j.wasman.2015.11.016.
[18] H. Duan, K.L. Hou, X. Zhu, Examining the technology acceptance for dismantling of waste printed circuit boards in light of recycling and environmental concerns, J. Environ. Manage. 92 (2011) 392.
[19] B. Wei, J.H. Li, H.H. Xie, Li-li Liu, Q.Y. Dong, Progress in research of comprehensive utilization of nonmetallic materials from waste printed circuit boards, Procedia Environ. Sci. 16 (2012) 500.
[20] R. Caymuil, R. Khanna, R. Rajarao, P.S. Mukherjee, V. Sahajwalla, Concentration of precious metals during their recovery from electronic waste, Waste Manage. (online) (2016), doi:http://dx.doi.org/10.1016/j.wasman.2015.12.004.
[21] I. de Marco, B.M. Caballero, M.J. Chomón, M.F. Laresgoiti, A. Torres, G. Fernández, S. Arnaiz, Pyrolysis of electrical and electronic wastes, J. Anal. Appl. Pyrolysis 82 (2008) 179.
[22] J. Moltó, S. Egea, J.A. Conesa, R. Font, Thermal decomposition of electronic wastes: Mobile phone case and other parts, Waste Manage. 31 (2011) 2546.
[23] T. Zhang, W.P. Walawender, L.T. Fan, M. Fan, D. Daugaard, R.C. Brown, Preparation of activated carbon from forest and agricultural residues through CO_2 activation, Chem. Eng. J. 105 (2004) 53.
[24] R.B. Rakhi, W. Chen, D. Cha, H.N. Alshareef, Nanostructured ternary electrodes for energy-storage applications, Adv. Energy Mater. 2 (2012) 381.
[25] M.D. Stoller, R.S. Ruoff, Best practice methods for determining an electrode material's performance for ultracapacitors, Energy Environ. Sci. 3 (2010) 1294.
[26] K.S.W. Sing, D.H. Everett, R.A.W. Haul, L. Moscou, R.A. Pierotti, J. Rouquerol, T. Siemieniewska, Reporting physisorption data for gas/solid systems with Special Reference to the Determination of Surface Area and Porosity, Pure Appl. Chem. 57 (1985) 603.
[27] K.S.K. Reddy, A.A. Shoaibi, C. Srinivasakannan, Activated Carbon from Date Palm Seed: Process Optimization Using Response Surface Methodology, Waste Biomass Valor. 3 (2012) 149.
[28] K. Jurewicz, K. Babel, A. Źiółkowski, H. Wachowska, Ammoxidation of active carbons for improvement of supercapacitor characteristics, Electrochim. Acta 48 (2003) 1491.
[29] N.M. Rodriguez, P.E. Anderson, A. Wootsch, U. Wild, R. Schlögl, Z. Páal, XPS, EM, and Catalytic Studies of the Accumulation of Carbon on Pt Black, J. Catal. 197 (2001) 365.
[30] J.P. Boudou, M. Chehimi, E. Broniek, T. Siemieniewska, J. Bimer, Adsorption of H_2S or SO_2 on an activated carbon cloth modified by ammonia treatment, Carbon 41 (2003) 1999.
[31] D. Hulicova-Jurcakova, M. Seredych, G.Q. Lu, T.J. Bandosz, Combined Effect of Nitrogen- and Oxygen-Containing Functional Groups of Microporous Activated Carbon on its Electrochemical Performance in Supercapacitors, Adv. Funct. Mater. 19 (2009) 438.
[32] C.O. Ania, V. Khomenko, E. Raymundo-Piñero, J.B. Parra, F. Béguin, The Large Electrochemical Capacitance of Microporous Doped Carbon Obtained by Using a Zeolite Template, Adv. Funct. Mater. 17 (2007) 1828.
[33] R. Rajarao, I. Mansuri, R. Dhunna, R. Khanna, V. Sahajwalla, Study of structural evolution of chars during rapid pyrolysis od waste CD at different temperatures, Fuel 134 (2014) 17.
[34] R. Rajarao, R. Ferreira, S.H.F. Sadi, R. Khanna, V. Sahajwalla, Synthesis of silicon carbide nanoparticles by using electronic waste as a carbon source, Mater. Lett. 120 (2014) 65.
[35] T. Lu, Y.P. Zhang, H.B. Li, L.K. Pan, Y.L. Li, Z. Sun, Electrochemical behaviours of graphene–ZnO and graphene–SnO_2 composite films for supercapacitors, Electrochim. Acta 55 (2010) 4170.
[36] Y. Yang, D. Kim, M. Yang, P. Schmuki, Vertically aligned mixed V_2O_5-TiO_2 nanotube arrays for supercapacitor, Chem. Commun. 2 (2011) 200.
[37] L.S. Aravinda, K.K. Nagaraja, H.S. Nagaraja, K. Udaya Bhat, B. Ramachandra Bhat, ZnO/carbon nanotube nanocomposite for high energy density supercapacitors, Electrochim. Acta 95 (2013) 119.
[38] R.B. Rakhi, H.N. Alshareef, Enhancement of the energy storage properties of supercapacitors using graphene nanosheets dispersed with metal oxide-loaded carbon nanotubes, J. Power Sources 196 (2011) 8858.
[39] A. Burke, R&D considerations for the performance and application of electrochemical capacitors, Electrochim. Acta 53 (2007) 1083.
[40] R. Kotz, M. Carlen, Principles and applications of electrochemical capacitors, Electrochim. Acta 45 (2000) 2483.
[41] D. Pech, M. Brunet, H. Durou, P. Huang, V. Mochalin, Y. Gogotsi, Ultrahigh-power micrometre-sized supercapacitors based on onion-like carbon, Nat. Nanotechnol. 5 (2010) 651.
[42] D. Kalpana, S.H. Cho, S.B. Lee, Y.S. Lee, R. Misra, N.G. Renganathan, Recycled waste paper—A new source of raw material for electric double-layer capacitors, J. Power Sources 190 (2009) 587.
[43] J. Mi, X.R. Wang, R.J. Fan, W.H. Qu, W.C. Li, Coconut-Shell-Based Porous Carbons with a Tunable Micro/Mesopore Ratio for High-Performance Supercapacitors, Energy Fuels 26 (2012) 5321.
[44] C. Peng, X. Yan, R. Wang, J. Lang, Y. Ou, Q. Xue, Promising activated carbons derived from waste tea-leaves and their application in high performance supercapacitors electrodes, Electrochim. Acta 87 (2013) 401.
[45] T.X. Shang, J. Zhang, F.L. Fan, X.J. Jin, Nitrogen-enriched activated carbons from waste particleboard used as electrode materials for supercapacitors: effects of activating agent on surface characteristics, RSC Adv. 5 (2015) 50843.
[46] J. Xu, Q. Gao, Y. Zhang, Y. Tan, W. Tian, L. Zhu, L. Jiang, Preparing two-dimensional microporous carbon from Pistachio nutshell with high areal capacitance as supercapacitor materials, Scientific Reports 4 (2014) 5545.